Chemical Engineering Journal 458 (2023) 141494

Contents lists available at ScienceDirect

Chemical Engineering Journal

journal homepage: www.elsevier.com/locate/cej

Comparison of the $NiAl_2O_4$ derived catalyst deactivation in the steam reforming and sorption enhanced steam reforming of raw bio-oil in packed and fluidized-bed reactors

Leire Landa *, José Valecillos, Aingeru Remiro, Beatriz Valle, Javier Bilbao, Ana G. Gayubo

Department of Chemical Engineering, University of the Basque Country (UPV/EHU), P.O. Box 644, Bilbao 48080, Spain

ARTICLE INFO

Keywords:
Raw bio-oil reforming
Hydrogen
CO_2 capture
Coke deactivation
Packed-bed reactor
Fluidized-bed reactor

ABSTRACT

The choice of appropriate reactors and reforming strategies is key to make progresses on scaling up H_2 production processes from raw bio-oil. This work compares the performance (conversion, product yields and deactivation) of packed-bed and fluidized-bed reactors (PBR and FBR, respectively) using a $NiAl_2O_4$ spinel derived catalyst for the H_2 production from raw bio-oil via steam reforming (SR) and sorption enhanced SR (SESR, with dolomite to capture CO_2). The experiments were carried out at 600 °C; steam/carbon ratio, 3.4; space time, 0.15 h; time on stream, 5 h; dolomite/catalyst ratio, 10 (SESR runs); and with prior thermal separation of the pyrolytic lignin from the raw bio-oil. The initial H_2 yields are 80 % and 69 % in the SR runs with PBR and FBR, respectively, and 99 % and 92 % in the CO_2 capture period (of 30 min duration) of the SESR runs in the PBR and FBR, respectively. The lower H_2 yield in the FBR is due to the less efficient gas–solid contact (bubbling or slugging phenomena). Based on the analysis of the spent catalysts with varied techniques the catalyst deactivation is related to the coke deposition, whose quantity and nature (amorphous or structured) depends on the reactor type and reforming strategy. The catalyst deactivation is slower in the FBR due to the rejuvenation of the catalyst surface by the moving particles that favor external coke gasification. The presence of dolomite prolongs the period of stable catalyst activity in both reactors with different effects on the coke quantity and nature. The results are of interest to advance on scaling up the SESR process that would require a FBR integrated with a regeneration unit for the catalyst and sorbent.

1. Introduction

Based on the increasing use of renewable sources (wind, solar, hydro, biomass, geothermal) a new energy economy, less carbon-intensive, is emerging, driven by political action, technological innovation and the growing urgency to address climate change [1]. Current use of hydrogen is covered by H_2 from fossil fuels (49 % from natural gas and 29 % from liquid hydrocarbons by steam reforming (SR), and 18 % from coal gasification), with significant associated CO_2 emissions [2–5]. In this scenario, the availability of green H_2 is considered key to reach the decarbonization targets of the energy system [2]. The routes of H_2 production from lignocellulosic biomass receive a great attention [3]. Among these routes, the steam reforming (SR) of raw bio-oil (obtained from fast pyrolysis of biomass) is considered an attractive and viable technology with a low environmental impact because of neutral CO_2 balance [6,7]. Raw bio-oil is a complex mixture of oxygenated organic compounds (acids, aldehydes, alcohols, carboxylic, ketones, esters, furfurals, phenolic and sugar-like compounds), which is obtained with a high yield from different types of lignocellulosic biomass, with simple equipment design (which can be used off-site) and low environmental impact [8,9]. Likewise, the SR of bio-oil avoids the costly dehydration of its high water content and enables the joint valorization of that contained in bio-oil [10].

The overall reaction for the SR of bio-oil (Eq. (1) in Table 1) involves reforming reaction to produce ($CO + H_2$) (Eq. (2)) and the subsequent water–gas-shift (WGS) reaction (Eq. (3)). According to Eq. (1), the maximum H_2 yield for the SR of bio-oil is ($2n + m/2 - k$) mol H_2/($mol_{oxygenates}$), but the real yield is lower due to the thermodynamic limitations of the WGS reaction and the existence of parallel secondary reactions, such as decomposition/cracking of oxygenates (Eq. (4)), reforming of decomposition products (CH_4 and light hydrocarbons (C_aH_b), Eqs. (5) and (6), respectively) and interconversion of oxygenates

* Corresponding author.
E-mail address: leire.landa@ehu.eus (L. Landa).

https://doi.org/10.1016/j.cej.2023.141494
Received 2 November 2022; Received in revised form 19 December 2022; Accepted 16 January 2023
Available online 18 January 2023

Table 1
Main and secondary reactions for the SR of bio-oil.

Global SR of bio-oil	$C_nH_mO_k + (2n-k)H_2O \rightarrow nCO_2 + (2n+\frac{m}{2}-k)H_2$	(1)
SR of bio-oil	$C_nH_mO_k + (n-k)H_2O \rightarrow nCO + (n+\frac{m}{2}-k)H_2$	(2)
Water-Gas-Shift (WGS)	$CO + H_2O \leftrightarrow CO_2 + H_2$	(3)
Oxygenates decomposition/ cracking	$C_nH_mO_k \rightarrow C_xH_yO_z + gas + C(coke)$ $gas = CO, CO_2, CH_4, C_aH_b, H_2$	(4)
Reforming of CH_4	$CH_4 + H_2O \leftrightarrow CO + 3H_2$	(5)
Reforming of light hydrocarbons	$C_aH_b + aH_2O \rightarrow aCO + (a + b/2)H_2$	(6)
Interconversion of oxygenates	$C_nH_mO_k \rightarrow C_xH_yO_z$	(7)
Methane decomposition	$CH_4 \rightarrow 2H_2 + C$	(8)
Boudouard reaction	$2CO \leftrightarrow C + CO_2$	(9)
Coke gasification	$C + H_2O \rightarrow CO + H_2$	(10)

(Eq. (7)). Moreover, the catalyst undergoes rapid and severe deactivation mainly due to coke deposition, whose amount depends on the relative importance of the reactions for its formation and gasification (Eqs. (8)-(10)).

Therefore, the challenges in the SR of bio-oil are focused on improving catalyst performance in order to increase H_2 yield and attenuate catalyst deactivation (coke formation and/or sintering) and on overcoming the thermodynamic limitation of the WGS reaction [11–14]. For this purpose, the use of a CO_2 solid sorbent together with the reforming catalyst (denoted sorption enhanced steam reforming, SESR) is an attractive strategy for H_2 production that improves the conventional SR for different feeds, as it increases H_2 yield and purity by shifting the equilibrium of the WGS reaction [15–19]. Moreover, SESR of bio-oil also contributes to making CO_2 sequestration easier, as it is released almost pure when the sorbent is regenerated, which has a remarkable techno-economic interest to contribute to energy decarbonization and reduction of emission taxes [20]. Therefore, the replacement of methane by bio-oil for H_2 production in refineries would be key to its sustainability [21]. Moreover, the exothermic carbonation reaction (ΔH_{298} = -178 kJ/mol, Eq. (11)) partially provides the energy required by the endothermic reforming reactions, contributing to mitigate its high-energy demand.

$$CaO + CO_2 \leftrightarrow CaCO_3 \quad (11)$$

The studies over catalyst development and reaction conditions (temperature, steam-to-carbon (S/C) molar ratio and space–time) in bio-oil SR have been performed mainly with Ni-based catalysts over different supports and with packed-bed reactors. The results evidence operating problems due to the rapid catalyst deactivation by coke, and even gas flow blockage when the feed is raw bio-oil [22,23]. Considering the relevance of catalyst deactivation by coke, it is required to be regenerable, recovering its activity after coke combustion. It has been demonstrated that a catalyst prepared by reduction of $NiAl_2O_4$ is completely regenerable [24] and its good performance in the reforming of bio-oil (with high activity, H_2 selectivity and stability) is due to the presence of highly dispersed and uniformly distributed Ni sites within the catalyst particle.

The scale-up of raw bio-oil SR or SESR (as well as other catalytic processes with high reaction heat and rapid catalyst deactivation) recommends the use of a fluidized-bed reactor [25], to avoid bed blockage problems [26,27] and the complex design and operation of packed-bed multitube reactors [28]. Thus, the free movement of the catalyst particles facilitates temperature control (uniform in the reactor and without cold or hot spots). Moreover, the high velocity of heat transport between phases facilitates heat input from the outside (needed because the reaction is highly endothermic). The movement of the catalyst in the fluidized-bed reactor would also facilitate the future operation of a reactor-regenerator system, with circulation of the catalyst between the two units, maintaining a constant catalyst activity in the reactor and continuously regenerating the catalyst (and the sorbent in the SESR operation). Papalas et al. [29] have simulated such a system for CH_4 reforming.

For the purpose of attenuating catalyst deactivation by coke, lower coke deposition has been observed in the fluidized-bed reactor compared to the packed-bed reactor in the steam reforming of biogas [30], acetic acid [31], aqueous fraction of bio-oil [26,32,33] and raw bio-oil [23], and in the oxidative reforming of ethanol [34]. The reason appears to be that the mixing regime of the catalyst particles, at a high temperature (above 600 °C in the experiments in the literature) and with the appropriate catalyst, promotes the gasification of the coke from bed particles and also delays the evolution of the coke towards structures that encapsulate the Ni sites.

However, results in the literature (in laboratory equipment or by simulation) show the negative effect of bubble presence in the gas–solid contact [35]. Thus, for the SR of methane [36], methanol [37], aqueous fraction of bio-oil [26,32] and raw bio-oil [23] the conversion is lower in the fluidized-bed reactor than in the packed-bed reactor. Fernández et al. [38] have studied the reforming of volatiles from biomass fast pyrolysis on a commercial Ni-Ca/Al_2O_3 catalyst attributing the higher coke deposition rate in the fluidized bed reactor to the higher concentration of unreacted oxygenates [39].

In this work, we compare the behavior of packed-bed and fluidized-bed reactors (hereafter PBR and FBR, respectively) in the SR and SESR of raw bio-oil. The objectives are: i) to evaluate the perspectives of using the FBR under the conditions required for the SESR (a moderate temperature to facilitate CO_2 sorption), comparing the results (evolution with time on stream of conversion and product yields) with those of the SR at the same conditions; ii) to identify the quantity and nature of the coke in both reactor types, and to evaluate the effect of the sorbent on these coke characteristics. A $NiAl_2O_4$ spinel-derived catalyst and dolomite as CO_2 sorbent have been used. The former has been selected due to its high activity and selectivity of H_2 in the raw bio-oil steam reforming and its full regeneration by coke combustion at 850 °C [24] and the latter because it is commonly used in SESR process due to its high sorption capacity, fast sorption kinetics and low cost [40–42]. The quantification of the deactivation and the knowledge of the coke nature for a real bio-oil feed in a fluidized-bed reactor is a relevant step to progress towards the scale-up of the SESR technology for the production of green H_2 from biomass minimizing CO_2 emissions.

2. Experimental

2.1. Preparation and characterization of catalyst and sorbent

The catalyst precursor (Ni-Al spinel, with a nominal Ni content of 33 wt%) was synthetized by co-precipitation method [43], by mixing aqueous solutions of *hexa*-hydrated nickel nitrate ($Ni(NO_3)_2{\cdot}6H_2O$, Panreac, 99 %) and aluminum nitrate nonahydrate ($Al(NO_3)_3{\cdot}9H_2O$, Panreac, 99 %) with a 0.6 M solution of ammonium hydroxide (NH_4OH, Fluka, 5 M) as a precipitating agent. The precipitation was carried out at 25 °C until the pH was fixed at 8. After aging for 30 min, the precipitate was filtered and washed with distilled water to remove the remaining ammonium ions. The recovered precipitate was dried at 110 °C for 24 h, calcined at 850 °C for 4 h and finally, crushed and sieved to obtain particle sizes in the range of 150–250 μm.

Natural dolomite ($CaMg(CO_3)_2$) produced and supplied by Calcinor S.A. (Cantabria, Spain) was used after the following treatment. Prior to each experiment, the as-received dolomite was dried at 110 °C for 12 h and calcined at 850 °C for 5 h with a heating ramp of 10 °C/min, so that the natural sorbent was thermally decomposed into CaO/MgO phases. Afterwards, it was sieved to ensure a particle size between 90 and 125 μm.

The quantitative composition of calcined dolomite (60.5 wt% CaO and 39.5 wt% MgO) was calculated by analysis of XRF data, performed

in a wavelength disperse X-ray fluorescence spectrometer (PAN-Analytical, AXIOS). The physico-chemical properties of the fresh-reduced and used catalyst samples were analysed by several techniques. The X-ray diffraction (XRD) analysis were conducted on a Bruker D8 Advance diffractometer with a CuKα1 radiation for determining the average Ni crystal size (using Scherrer equation) and the crystalline state of coke deposits. The specific surface area (BET), pore volume and average pore diameter were determined by adsorption–desorption of N_2 in a Micromeritics ASAP 2010. The scanning electron microscopy (SEM) images of the fresh or used catalysts were obtained in a Hitachi S-4800 N field emission gun scanning electron microscope with an accelerating voltage of 5 kV and secondary electron detector (SE-SEM) and a Hitachi S-3400 N microscope with an accelerating voltage of 15 kV using a backscatter electron detector (BSE-SEM). The content, nature and location of the total coke deposited in the catalyst and sorbent was analyzed by Temperature Programmed Oxidation (TPO) in a TA-Instruments TGA-Q5000IR thermobalance, coupled in line with a Thermostar Balzers instrument mass spectrometer for monitoring the CO_2 signal. The TPO profile was quantified from the CO_2 spectroscopic signal, because the oxidation of Ni crystals during coke combustion masks the thermogravimetric signal. The Raman spectra were carried out in a Renishaw InVia confocal microscope using an excitation wavelength of 514 nm, taking a spectrum in several areas of the sample for assuring reproducibility.

2.2. Bio-oil production and composition

The raw bio-oil (supplied by BTG Bioliquids BV, The Netherlands) was obtained by flash pyrolysis of pine sawdust in a plant provided with a conical rotatory reactor (RCR) with a capacity to operate continuously with 5 t/h of biomass. The chemical composition was determined by gas chromatography/mass spectrometry (GC/MS) analysis on a Shimadzu GC/MS-QP2010S, provided with a BPX-5 column, with a length of 50 m, diameter of 0.22 m and thickness of 0.25 μm, and a mass selective detector. The identification of the compounds was carried out by comparison with the pattern spectra available in NIST 147 and NIST 27 library. The detailed composition is described elsewere [44], and it is gathered in Table S1 of Supplementary Material. The main components are acetic acid (16.6 wt%), levoglucosane (11.1 wt%), guaiacol (11.1 wt %) and acetol (9.4 wt%). The water content (24 wt%) was determined by Karl Fischer volumetric valorization (KF Titrino Plus 870). The empirical formula ($C_{4.6}H_{6.2}O_{2.4}$) was obtained by CHO analysis in a Leco CHN-932 analyzer (water-free basis).

2.3. Reaction equipment, operating conditions and reaction indices

The SR and SESR experiments were performed in an automatized reaction equipment (MicroActivity-Reference, PID Eng & Tech) provided with two units in series for thermal treatment of raw bio-oil (Unit 1) and catalytic reforming (Unit 2) of treated bio-oil [43]. The first unit is a U-shaped steel tube (inner diameter = 0.75 in) at 500 °C for vaporization of bio-oil and controlled deposition of pyrolytic lignin (PL) formed by repolimerization of oxygenates (mainly phenolic compounds), which is responsible for rapid catalyst deactivation [45]. Consequently, the catalyst deactivation is noticeably attenuated using this reaction system with two steps in series [46]. In a previous work [47], it was proved that 500 °C is the thermal treatment temperature that allows obtaining a better compromise between the yield of liquid volatiles susceptible to be reformed in subsequent Unit 2 (treated bio-oil), of solid deposited as PL and of gases. With the bio-oil feed used in this work, the yield (dry basis) of treated bio-oil, PL and gases is 75 wt %, 15 wt% and 10 wt%, respectively. The composition of the treated bio-oil has been detailed in Table S1 of Supplementary Material. The gases consist mainly of CO (56.1 wt%) and CO_2 (25.5 wt%) resulting from oxygenates decarbonylation/decarboxylation reactions, and with low concentration of H_2 (1.3 wt%), CH_4 (7.7 wt%) and C_2-C_3 hydrocarbons (9.5 wt%) resulting from decomposition/cracking reactions of the oxygenates. The second unit is a stainless-steel tube (22 mm of internal diameter, total length of 460 mm and effective reaction length of 10 mm), for the reforming of the volatiles exiting Unit 1 (treated bio-oil), which is operated with downwards (PBR) or upwards (FBR) flux. The catalytic bed is located over a layer of quartz wool and consists of the catalyst mixed with inert solid (SiC, with particle size of 75 μm), in order to improve the isothermal condition (in packed-bed) and the fluid dynamics (in the fluidized-bed) of the bed. An injection pump (Harvard Apparatus 22) was used for feeding the bio-oil (0.06 ml/min) and a 307 Gilson pump for co-feeding the additional water required according to the desired steam to carbon (S/C) molar ratio. The reaction products were analyzed in a Micro GC Varian CP-490 connected in-line to the reactor through an insulated line (130 °C) to avoid condensation of the products, and equipped with three analytic channels: molecular sieve MS5 for quantifying H_2, O_2, N_2, CH_4 and CO; PPQ column for light hydrocarbons (C_2-C_4), CO_2 and water; and Stabilwax for oxygenated compounds (C_{2+}) and water. Prior to each reaction, the $NiAl_2O_4$ spinel is reduced in situ under H_2-N_2 (10 vol% H_2) at 850 °C for 4 h, thus obtaining the active Ni metallic phase well-dispersed on the support of alumina. The experiments were carried out at atmospheric pressure and 600 °C, with S/C of 3.4 and space–time of 0.15 $g_{catalyst}h/g_{oxygenates}$ These values of temperature and S/C ratio were chosen based on a previous work [12] in which the effect of operating variables in the SR of bio-oil over this catalyst in a fluidized-bed reactor was studied. These values provide the best compromise of activity - H_2 selectivity - catalyst stability. Moreover, the space–time is low enough to appreciate the deactivation of the catalyst in a short reaction time. In the SESR runs, a sorbent/catalyst mass ratio of 10 was used. In both reactor types inert gas (N_2) was co-fed with the bio-oil and water, so that the linear gas velocity (u) is 4.3 cm/s. For this conditions, in the fluidized-bed reactor the linear gas velocity is 6 times the minimum of fluidization ($u_{f,min}$), which was experimentally determined (by pressure drop evolution). Under these conditions, bed stagnation and segregation of catalyst and sorbent are avoided.

The catalyst performance was quantified according to the conversion of oxygenates in the treated bio-oil (that is, the volatiles oxygenates exiting the Unit 1 for thermal treatment) (Eq. (12)), H_2 yield (Eq. (13)), and yield of carbon products (CO_2, CO, CH_4, and hydrocarbons) (Eq. (14)):

$$X = \frac{F_{out,\ gas}}{F_{in}} \cdot 100 \tag{12}$$

$$Y_{H_2} = \frac{F_{H_2}}{F^{o}_{H_2}} \cdot 100 \tag{13}$$

$$Y_i = \frac{F_i}{F_{in}} \cdot 100 \tag{14}$$

According to Eq. (12), the oxygenates conversion is expressed as the carbon units converted into gas. In these equations, $F_{out,gas}$ is the carbon-based molar flow rate of the carbonaceous gaseous product (CO_2, CO, CH_4 and light hydrocarbons) at the reactor outlet; F_{in} is the carbon-based molar flow rate of oxygenates at the reactor inlet; F_{H2} is the H_2 molar flow rate in the product stream; $F^{o}_{H_2}$, is the stoichiometric molar flow rate, which is calculated as $(2n + m/2 - k)/n\ F_{in}$, according to the global stoichiometry for the bio-oil ($C_nH_mO_k$) steam reforming (Eq. (1), including the WGS reaction), and F_i is the carbon-based molar flowrate of the i product (CO_2, CO, CH_4 and hydrocarbons) in the effluent (out) stream of the reactor. Coke yield has been quantified referring the total amount of coke deposited at the end of the reaction to the total mass of C at the reactor inlet.

3. Results

3.1. Performance of the packed and fluidized-bed reactors

The influence of using a PBR or FBR on the behavior of $NiAl_2O_4$ spinel derived catalyst in the SR or of the pair dolomite/catalyst in the SESR of bio-oil is compared in this section.

3.1.1. Steam reforming.

Fig. 1 shows the evolution with time on stream (TOS) of the conversion and product yields obtained in the PBR (full markers) and FBR (empty markers) in the absence of CO_2 sorbent (conventional SR). The comparison of the results in both reactors show a higher initial stability in the PBR, in which the conversion and H_2 and CO_2 yields remain almost constant along 120 min. (Fig. 1a), and are close to the thermodynamic equilibrium. Thus, according to prior studies [48,49], at 600 °C and S/C of 3.4 (this being the S/C ratio resulting in the treated bio-oil, once subtracted the PL deposited in Unit 1 during the thermal treatment) in the thermodynamic equilibrium the oxygenates conversion is complete and the yields of H_2 and CO_2 are 82.3 % and 73.4 %, respectively. Nevertheless, subsequently they rapidly decrease due to catalyst deactivation for the WGS (Eq. (3)) and reforming (Eq. (2)) reactions. The increase of light hydrocarbons yield after 120 min in Fig. 1b can be explained because the extent of its forming reaction (oxygenates cracking/decomposition reaction, Eq. (4)) is favored by the increase of oxygenates concentration as the catalyst is deactivated, and by the deactivation of their reforming reaction (Eq. (6)). Interestingly, the yields of CO and CH_4 (intermediate compounds in the overall reaction scheme (Eqs. (1)-(10)) remain almost constant with TOS, which suggests that their forming and disappearing reactions are similarly affected by the catalyst deactivation [12].

In the FBR (empty markers in Fig. 1) there are lower initial values of conversion and H_2 and CO_2 yields (Fig. 1a) and higher CH_4 yield (Fig. 1b) than in the PBR due to the less effective gas–solid contact. Moreover, an initial steady period of complete carbon conversion in the reforming reactions is not observed in the FBR, so that the carbon conversion and the yields of H_2 and CO_2 decrease from the beginning of the reaction. Therefore, H_2 yield is initially lower and decreases more rapidly at the beginning of the reaction in the FBR (probably due to the higher concentration of unreacted oxygenates, which are the main precursors of coke by decomposition/cracking) [39]. However, the deactivation rate is slower in the FBR than in the PBR with increasing TOS, and a similar H_2 yield is achieved after 300 min TOS, around 41 %. This lower deactivation in the FBR is in agreement with the results in the literature on biogas reforming [30], pure oxygenates [31], aqueous fraction of bio-oil [26,32,33] and raw bio-oil [23].

As explained in section 3.2, these different deactivation trends in both reactors is consequence of the complexity of the coke formation mechanism, which depends on the evolution with TOS of the extent of its formation reactions (Eqs. (4), (8) and (9)) and its removal by gasification (Eq. (10)). Moreover, as established in the literature [50–52], the nature of the coke formed at different reaction steps (Eqs. (4), (8) and (9)) is different and has a different impact on catalyst deactivation. The gas–solid contact regime, which is different in both reactors, and the movement of the catalyst particles in the fluidized reactor will have an impact on the extent of these coke formation reactions.

Fig. 1b shows that in FBR, hydrocarbons yield remains nearly null, which evidences a slow deactivation of their reforming reaction (Eq. (6)), whereas CO yield slightly increases and CH_4 yield decreases with TOS, evidencing that catalyst deactivation also affects the WGS reaction (Eq. (3)) and methane forming reactions (Eq. (4) and reverse Eq. (5)) [12,43].

3.1.2. Sorption enhanced steam reforming.

Fig. 2 compares the performance along TOS of the PBR and FBR in the SESR runs. In the initial CO_2 capture period, whose duration is almost 30 min in both reactors, the H_2 yield is almost 100 % in PBR run and 92 % in FBR (Fig. 2a). In this period, complete oxygenate conversion is achieved in PBR, and the conversion to gas is near zero because the yields of CO, CH_4 and hydrocarbons are almost null (Fig. 2b).

After the saturation of dolomite, in the PBR (full makers) the conversion is almost complete up to 160 min TOS, with high H_2 and CO_2 yields (80 % and 70 %, respectively). In this period the CO yield is around 17 % and CH_4 yield is low (3–4 %). Moreover, the hydrocarbons formation (Fig. 2b) is null, and there is even longer duration of the stable period than in the SR run (Fig. 1a). Subsequently, the conversion and yields of H_2 and CO_2 sharply decrease, which evidences a rapid catalyst deactivation for the reforming of oxygenates and of CH_4 and hydrocarbons, whose yields increase after 180–240 min TOS. CO yield keeps quite constant, which points to a similar deactivation rate of the reactions of CO formation and conversion. In the FBR (empty markers in Fig. 2), the yields of H_2 and CO_2 after dolomite saturation are lower than in the PBR, coherently with the results obtained in the SR runs (Fig. 1). Interestingly, a short stable period (around 40 min) with almost constant yields is observed, that could be attributed to the activity of dolomite, so that the reactor operates initially which excess of active sites for oxygenates conversion (thus partially overcoming the less effective gas–solid contact in the fluidized-bed). Nevertheless, the decrease in

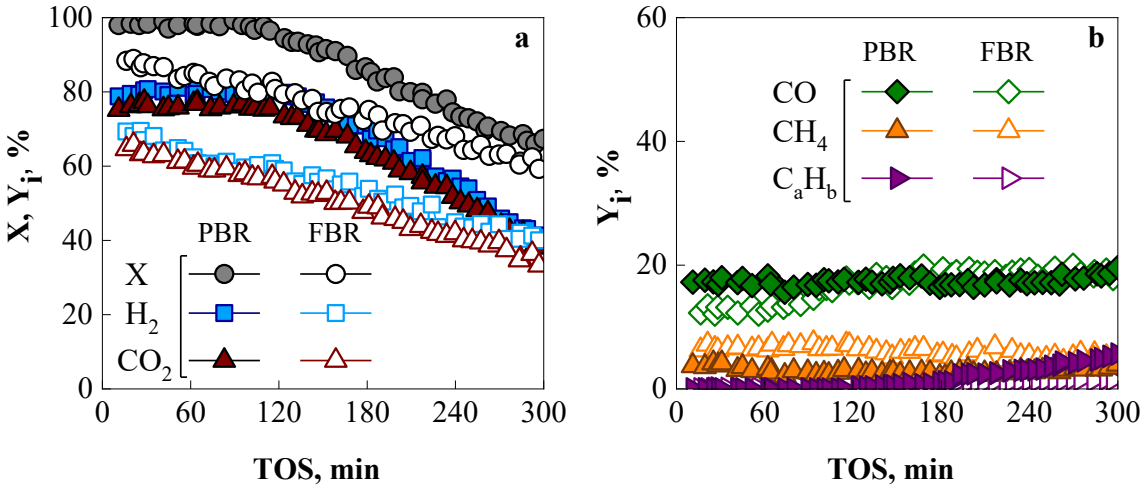

Fig. 1. Evolution with time on stream (TOS) of the conversion and H_2 and CO_2 yields (a) and CO, CH_4 and hydrocarbons yields (b) in the SR runs in PBR (full markers) and FBR (empty markers).

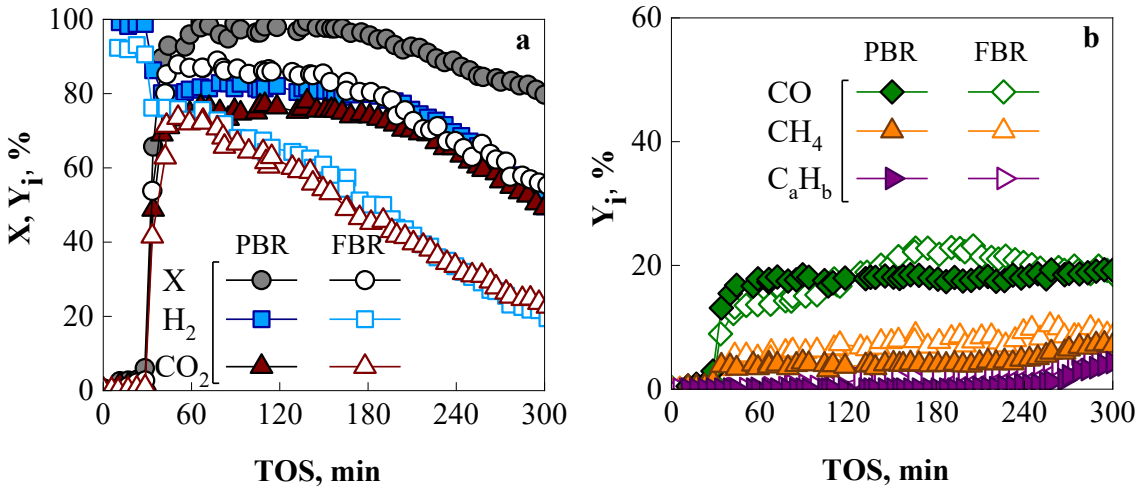

Fig. 2. Evolution with time on stream (TOS) of the conversion and H_2 and CO_2 yields (a) and CO, CH_4 and hydrocarbons yields (b) in the SESR runs in PBR (full markers) and FBR (empty markers).

conversion and in the yields of H_2 and CO_2 in the FBR (Fig. 2a) is faster in the presence of dolomite than in the SR run without dolomite (Fig. 1a).

In view of the aforementioned results, in the CO_2 sorption stage, the presence of dolomite significantly modifies the product distribution in both beds, allowing obtaining almost pure H_2. In the post-saturation stage, the presence of dolomite seems to have two opposite effects on the catalyst deactivation in both fluid dynamic regimes. On the one hand, it enlarges the duration of the pseudo-stable period compared to the SR runs without dolomite, which could be explained by the dolomite activity for the conversion of oxygenates by reforming (Eq. (2)), interconversion (Eq. (7)) and decomposition/cracking (Eq. (4)) reactions [53]. On the other hand, the presence of dolomite originates a faster deactivation of the catalyst, so that after the pseudo-stable period there is a more rapid decrease in the carbon conversion and yields of H_2 and CO_2 than in the SR run without dolomite. This fact suggests that the presence of dolomite has a negative impact on deactivation which is greater than its positive role of acting as a catalyst guard, retaining on its surface a fraction of the coke (in particular that related to pyrolytic lignin and predominantly deposited on the external surface of the dolomite and catalyst particles) [54].

The comparison of the results in the PBR and FBR for the SR and SESR of raw bio-oil shows the importance of the fluid dynamic regime of the reactor on the conversion of oxygenates, product yields and their evolution with TOS. The less effective gas-catalyst contact occurring in the FBR explains the lower initial carbon conversion and yields of H_2 and CO_2, as reported in literature in the SR of different feeds [23,26,32,36–38]. As a consequence, coke deposition is favored due to the higher concentration of oxygenates (coke precursors by decomposition/cracking reactions (Eq. (4))), although this effect will be partially mitigated by the "catalyst rejuvenation", due to the movement of the particles that favors their contact with the gas stream, promoting gasification and attenuation of coke evolution. This phenomenon, with notable incidence at high temperatures in the reforming of different feeds [23,26,30–33], will have a lower effect at 600 °C (temperature required for CO_2 sorption, but insufficient to promote the efficient gasification of the coke).

In next section, we present the results of the characterization of catalyst used samples and of deposited coke in order to better understand the reasons for the differences in catalyst deactivation in both reactors in the SR and SESR runs.

3.2. Characterization of used catalyst and coke

The deactivated catalyst samples have been characterized with different techniques (described in section 2.1) in order to ascertain the effect of the fluid-dynamic regime of the reactor and the role of using dolomite as a CO_2 sorbent on the possible causes of deactivation. These causes include: i) deposition of coke on the catalyst surface (amount and characteristics of coke deposits), ii) changes in Ni oxidation state and crystal size, and iii) aging and clogging of the support.

It should be noted that after each reaction, the solids composing the catalytic bed were separated by sieving, to avoid masking the characterization of the used catalyst by the presence of the other solids (inert in the SR runs or inert/sorbent in the SESR runs). The particle size selected for each solid (SiC, 50–90 μm; dolomite 90–125 μm; catalyst 150–250 μm) facilitates this separation. Thus, only traces of inert or dolomite might remain in the used catalyst after sieving.

3.2.1. Structural properties.

Fig. 3 shows the X-ray diffraction (XRD) patterns of fresh (reduced) and deactivated catalysts samples used in the SR and SESR runs with PBR or FBR. In the fresh (reduced) catalyst, peaks corresponding to Ni^0 (44.6°, 51.8° and 76.3° diffraction angels) (PDF 04-010-6148) and Al_2O_3 (37.5°, 45.9° and 66.9° diffraction angels) (PDF 04-005-4662) have been identified. The same peaks were observed for deactivated catalysts. Moreover, in the used sample in PBR-SR run the peak at 35.7° corresponds to SiC (PDF 00-031-1232), and in the diffractogram of PBR-SESR sample the peaks at 29.3 and 35.6° correspond to $CaCO_3$ (PDF 01-086-2340). The presence of these latter peaks is due to traces of inert solid (SiC) or sorbent (dolomite) resulting in the separation by sieving of the catalytic bed solids, which is necessary to obtain the spent catalyst samples. The presence of NiO (PDF 01-080-5508) was not detected in the XRD results of any deactivated sample, in agreement with H_2-TPR (results not shown). Therefore, metal oxidation was ruled out as deactivation cause. The absence of oxidized species is due to the highly reducing environment in both SR and SESR runs, with high H_2 content.

The average Ni^0 particle size (Table 2) were calculated using Debye-Scherrer equation at $2\theta = 51.8°$ (Ni^0 (200) plane), in order to assess the sintering of Ni crystals. The similar average size of Ni^0 crystals in Table 2 for the fresh (reduced) and used catalysts (15 nm and 16–20 nm, respectively) in both reactors, shows no evidence of a noticeable degree of sintering of Ni crystals. Therefore, sintering phenomenon was also excluded as a possible cause of deactivation at the reaction conditions tested at this work.

XRD patterns of the deactivated catalyst samples also provide

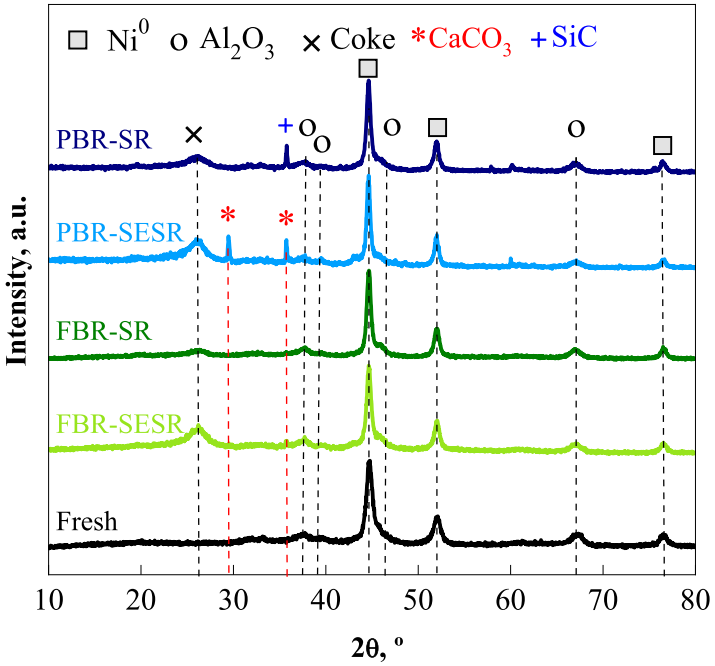

Fig. 3. X-ray diffraction (XRD) patterns of fresh (reduced) and deactivated catalyst samples used with a PBR or FBR in the SR and SESR of raw bio-oil runs.

Table 2
Physico-chemical properties (average Ni^0 crystal size (d_{Ni}), S_{BET}, V_{pore} and d_{pore}) of fresh (reduced) and deactivated catalyst used in the SR and SESR of raw bio-oil with PBR or FBR.

Catalyst	Reactor type	Run	d_{Ni} (nm)	S_{BET} (m^2/g)	V_{pore} (cm^3/g)	d_{pore} (nm)
Fresh (reduced)	–	–	15	65.1	0.24	13.1
Deactivated	PBR	SR	17	64.2	0.17	12.9
		SESR	20	43.2	0.12	17.0
	FBR	SR	17	72.8	0.18	9.4
		SESR	16	69.6	0.18	13.4

information on the coke deposits. The presence of a broad peak at a diffraction angle $2\theta = 26°$ (PDF 00-026-1080) for the catalyst used in PBR in SR conditions suggests the presence of a high crystallinity coke (graphitic carbon), which is less observable for that used in FBR. Moreover, the use of dolomite increases the intensity of this diffraction peak in both reactors, which indicates the presence of more crystalline carbon structures.

Ruling out Ni oxidation and sintering as causes of deactivation, this must be attributed to coke deposition. The deposition of different types of coke (inside and outside the particles) causes the deterioration of the catalyst properties, leading to a partial blocking of the pores of the Al_2O_3 support, which together with the encapsulation of the Ni sites by amorphous coke are the causes of catalyst deactivation [45,55]. To evaluate the deterioration of the porous structure of the catalyst, N_2 adsorption–desorption isotherms (Fig. S1, with the respective description of the isotherms) have been obtained for fresh (reduced) and deactivated catalysts samples, from which the textural properties (BET surface area, average pore diameter and pore volume) have been calculated (Table 2). For the SR runs, the increase in BET surface area for the catalyst deactivated in FBR (72.8 $m^2\ g^{-1}$) compared to that of the fresh (reduced) catalyst (65.1 $m^2\ g^{-1}$) suggests the presence of a porous coke structure, as that corresponding to filamentous carbon. Nevertheless, the BET surface area of the catalyst used in the PBR (64.2 $m^2\ g^{-1}$) is slightly lower than that of the fresh (reduced) catalyst. This result evidences a different morphology of coke formed in the PBR than in the FBR.

Conversely, the BET surface area of the catalyst used in PBR and the pore volume of the catalysts used in both PBR and FBR decrease with the presence of dolomite (SESR runs) which suggests a partial blockage of the mesoporous structure of Al_2O_3 support according to the deposition of additional low porosity coke (amorphous carbon), which is more noticeable in the PBR. The slight increase in BET surface area observed in the catalyst used in the SESR run in the FBR compared to the fresh catalyst could be explained by additional porosity created by some filamentous coke deposited on this sample, which partially counteracts the decrease in BET surface area due to amorphous coke. Concerning the average pore diameter, there is no trend with the use of dolomite.

3.2.2. *Morphology and location of coke*

Backscattered electron (BSE-SEM) detector was used to distinguish between different elements on the external surface of the catalyst particles based on the brightness intensity, which depends on the atomic number of the compounds [52]. The brightest level indicates the presence of heavy elements such as Ni and Al (constituting the Ni crystals and Al_2O_3 support), whereas the darkest intensity indicates the presence of light components such as C (for coke). Thus, Fig. 4 shows the fresh

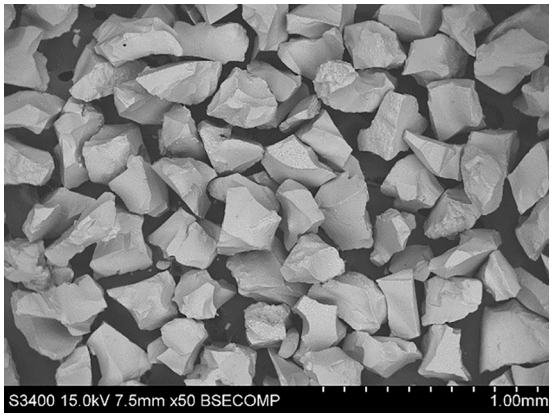

Fig. 4. BSE-SEM image of fresh (reduced) catalyst.

(reduced) catalyst particles, where the high brightness intensity reveals merely the presences of heavy compounds. On the other hand, Figs. 5 and 6 display deactivated catalyst particles used in the SR or SESR runs, respectively, with the two different reactors. In comparison with the fresh catalyst, all the used samples exhibit a low brightness intensity (dark appearance), which indicates the carbon deposition on the particle external surface. Based on the brightness intensity, in the absence of dolomite (SR runs) carbon deposition is more severe on the catalyst used in a PBR (Fig. 5a) than on that used in the FBR (Fig. 5b). The latter shows a homogeneous higher brightness level, which evidences less coke deposition on the external surface of the particle.

Nonetheless, the use of dolomite (Fig. 6) results in a heterogeneous coke deposition, showing differences in the particle shapes and textures for both reactors. In the PBR (Fig. 6a) the agglomeration of catalyst particles embedded in coke agglomerates can be seen, whereas the particles used in the FBR are separated, with the presence of abundant carbonaceous material on their surface (Fig. 6b).

In order to ascertaining the coke morphology in more detail, SE-SEM images of the catalysts particles zoomed in on the catalyst surface are shown in Fig. 7 (fresh catalyst), 8 (used in SR runs) and 9 (used in SESR runs). The typical particles of the fresh (reduced) catalyst show a uniform granular texture (rough and porous structure), which is expected for porous alumina phases [56]. In some particles of the sample used in the FBR (those with dark rough surface in Fig. 5b) the presence of mostly thin, loose and short carbon filaments is observed (Fig. 8b). Nevertheless, most of the catalyst particles used in FBR (slight bright smooth particles in Fig. 5b) show a porous surface resembling that of the fresh catalyst (Fig. S2 in Supplementary Material), evidencing a low carbon deposition on their external surface. In the catalyst used in PBR (Fig. 8a) some carbon filaments are also observed, which are more heterogeneous than those formed in the fluidized-bed, and interestingly, abundant carbon spheres are formed. In the catalyst used in the SESR run in PBR (Fig. 9a) the presence of carbon spheres is lower, being higher the presence of carbon filaments as in the catalyst used in the FBR (Fig. 9b). This higher amount of carbon filaments deposited on the catalysts samples used in the SESR runs compared to SR runs is coherent with the observation of more crystalline coke structures in the XRD diffractograms of these samples (Fig. 3).

3.2.3. *Amount and types of coke*

The amount of coke deposited on the catalyst and on dolomite and its nature and/or location in the particle have been determined by TPO analysis of the used materials. Fig. 10 shows the TPO profiles of the catalyst used in the SR (Fig. 10a) and SESR (Fig. 10b) runs with both reactor configurations (PBR and FBR). In terms of total coke contents (Table 3), a lower amount is observed in the catalyst used in FBR, compared to the one used in PBR. Thus, in the SR run this difference is considerable and the contents are 73 wt% and 17 wt% for PBR and FBR, respectively. This difference, smaller in the SESR runs, is in agreement with the higher pore blockage and decrease of the BET surface area in the PBR (Table 2). This result is coherent with the established effect of particle movement in the FBR on attenuating coke formation in the reforming of different feeds [26,30–33].

The comparison of the average coke yields on the catalyst after 300 min TOS (Fig. 11) shows that it decreases with the presence of dolomite in the PBR, but conversely increases in the FBR. The coke yield deposited on dolomite in the SESR runs (3.7 % and 2.9 % in PBR and FBR, respectively, Fig. 11) highlights the coke-forming capacity of dolomite, and suggest that the vigorous contact between catalyst and dolomite in the FBR (with dolomite/catalyst ratio of 10) favors the mechanisms of coke formation on the catalyst. This coke-forming capacity of dolomite has been demonstrated in previous works [53,54] in which dolomite has been used as a guard-bed prior to the reforming reactor due to its capacity for the pre-reforming of oxygenates from the bio-oil, so that it modifies the composition of the oxygenates and enables the extent of the reforming in the subsequent reforming step.

In all the TPO profiles in Fig. 10 two combustion domains are identified, which are characteristic in the reforming of different feeds such as volatiles from plastics pyrolysis [51,52,57], toluene or biomass tar [58–60] and oxygenates in bio-oil [45,50,52] and is attributable to different coke nature: a fraction burning at low temperature, with the maximum of its combustion peak below 500 °C (LT-coke), which is of amorphous nature and is deposited on or near the Ni sites, which facilitates its combustion and; a fraction burning at high temperature, (HT-coke) formed by structured carbon (graphitic or filamentous carbon) most probably deposited over Al_2O_3 support. These TPO profiles are in line with the XRD diffractograms in Fig. 3, showing low peak intensity at $\theta = 26°$ (corresponding to coke crystalline structures) in the sample deactivated in the SR run in FBR (whose HT-coke fraction is minority). Furthermore, the comparison of the results of coke morphology (section 3.2.2) with those of coke content and combustion characteristics (Fig. 10) evidences that there is a direct correlation between HT-coke fraction and the coke that is clearly visible on the catalyst external surface. Thus, most of the deactivated catalyst particles in the SR run in FBR (with minority formation of HT-coke, Fig. 10a), are bright (Fig. 5b).

The TPO profiles in Fig. 10 have been deconvoluted into several combustion peaks, and those with the maximum of the peak located below 500 °C have been assigned to LT-coke, whereas those with maximum of combustion peak above 500 °C are assigned to HT-coke. The results of the deconvolution of the TPO profiles of the catalyst used in the SR run in PBR (Table 3), evidence that HT-coke is the prevailing coke fraction in this sample (89.2 % of the total coke), whose combustion peak has a maximum at 560 °C (Fig. 10a). When dolomite is used in the PBR (SESR runs), HT-coke formation decreases and its combustion peak shifts towards lower combustion temperature

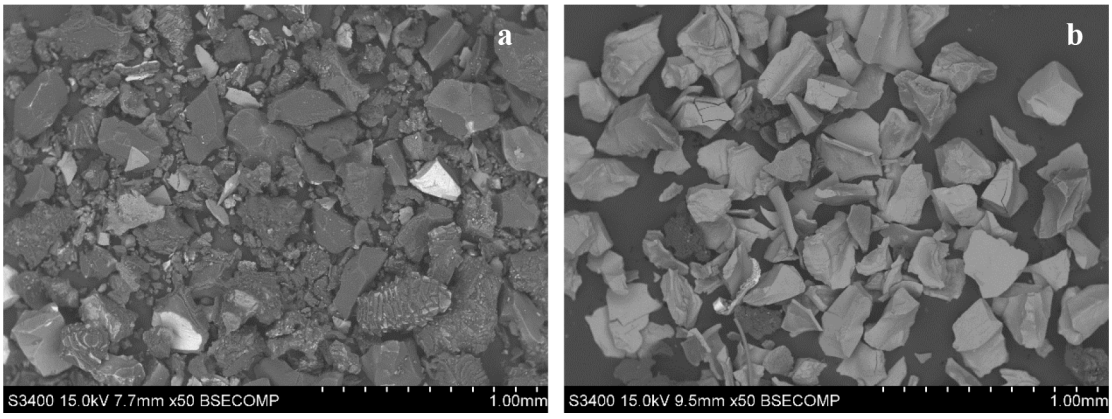

Fig. 5. BSE-SEM images of the catalyst used in the SR runs in PBR (a) and FBR (b).

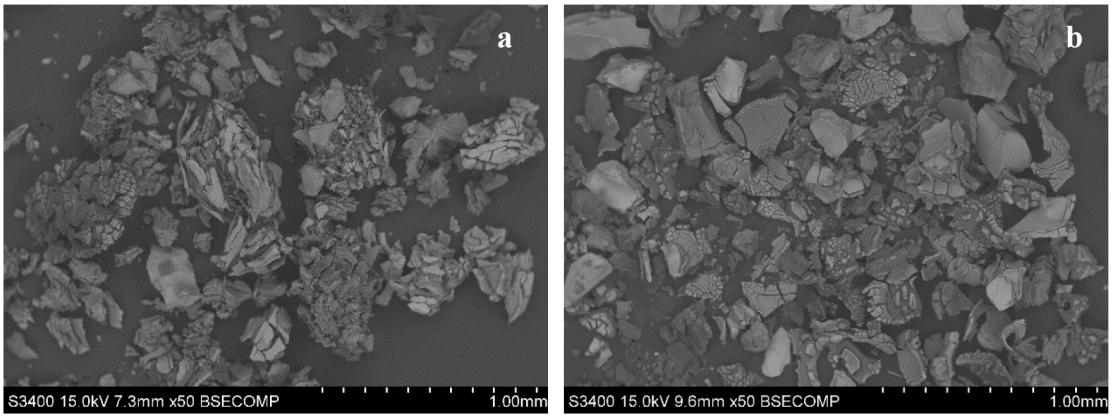

Fig. 6. BSE-SEM images of the catalyst used in the SESR runs in PBR (a) and FBR (b).

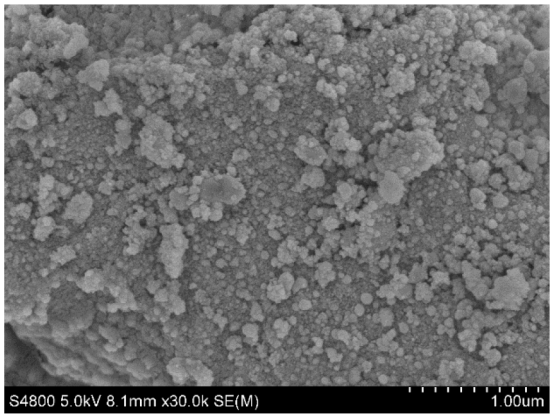

Fig. 7. SE-SEM image of fresh (reduced) catalyst.

(538 °C), whereas the growth of the LT-coke fraction is promoted (Fig. 10b). As a result, the HT-fraction is 76.7 % of the total coke.

The relative content of coke fractions in the catalyst used in SR run with FBR (dashed lines in Fig. 10a) differs significantly from that used in the PBR (solid lines). Thus, in the FBR the formation of HT-coke (5.0 wt %, Table 3) is noticeably attenuated compared to the PBR (64.7 wt%) and it burns at higher temperature (maximum at 587 °C), which suggests that it is more structured coke. This may be a consequence of the favored gasification of HT-coke in the FBR, that noticeable reduces its amount, but leaves a carbon structure that is more condensed/developed. Nevertheless, the content of LT-coke (12.2 wt%) is slightly higher than in the PBR (7.9 wt%), most probably due to the lower conversion and, consequently, higher concentration of oxygenates, which are precursors of the amorphous LT-coke formation by decomposition/cracking reaction (Eq.(4)). Conversely, in the presence of dolomite (SESR runs, Fig. 10b), the formation of HT-coke is predominant (43.9 wt%, 76.3 % of the total coke) over LT-coke (content of 13.6 wt%).

The different evolution observed in the formation of both coke fractions due to the presence of dolomite seems to indicate a change in the mechanism of coke formation, and this variation is affected differently by the fluid dynamic regime in the reactor. The possible cause of this change may be the role of dolomite as a catalyst for the interconversion reactions of the oxygenated in the bio-oil [53]. Consequently, changes in the composition of the oxygenates will have a major impact on coke formation and nature, as has been demonstrated [44]. In the FBR, a synergy between the mechanisms of coke formation on both solids cannot be ruled out, so that the deposition of amorphous coke on dolomite (exclusive because no HT-coke is formed, as shown in Fig. S3 of Supplementary Material) favors the development of the mechanism of coke formation and evolution on the catalyst, due to the vigorous contact between the catalyst and dolomite particles in this reactor. Another plausible explanation is the water adsorption capacity of saturated dolomite ($CaCO_3$ + MgO), considering that $CaCO_3$ is able to adsorb water at high temperatures [61]. Although the water adsorption capacity of the saturated dolomite (0.017 and 0.010 mmol/g at 150 °C and 400 °C, respectively) is lower than that of the catalyst (0.096 and 0.031 mmol/g at 150 °C and 400 °C, respectively), the presence of a large amount of dolomite in the catalytic bed (dolomite/catalyst ratio of 10) may cause a water adsorption competition with the catalyst, which negatively affects the coke gasification.

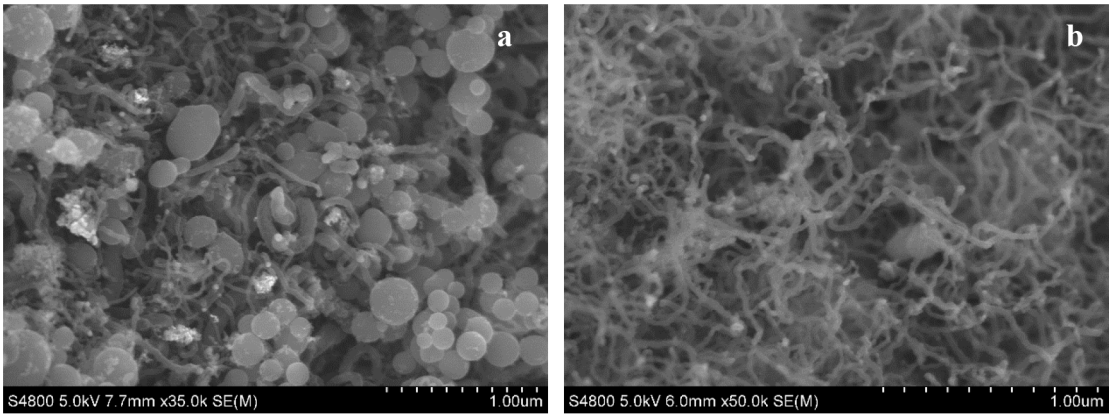

Fig. 8. SE-SEM images of the catalyst used in the SR runs in PBR (a) and FBR (b).

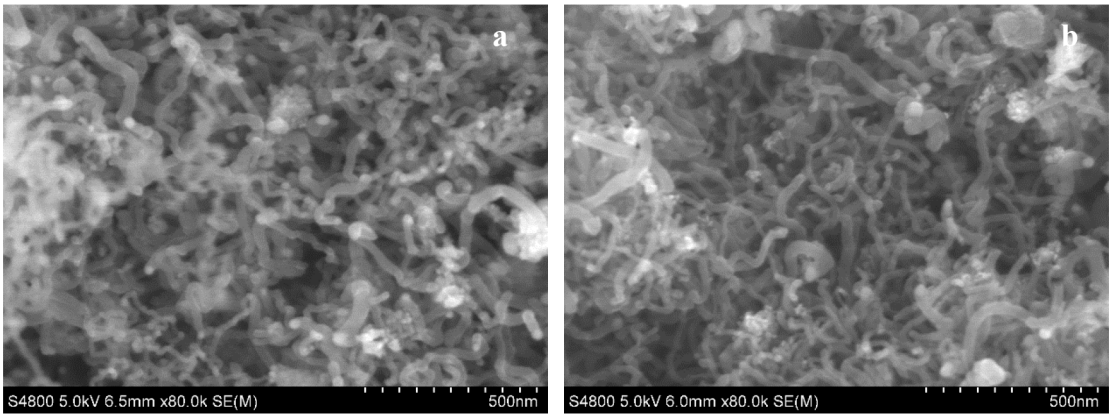

Fig. 9. SE-SEM images of the catalyst used in the SESR runs in PBR (a) and FBR (b).

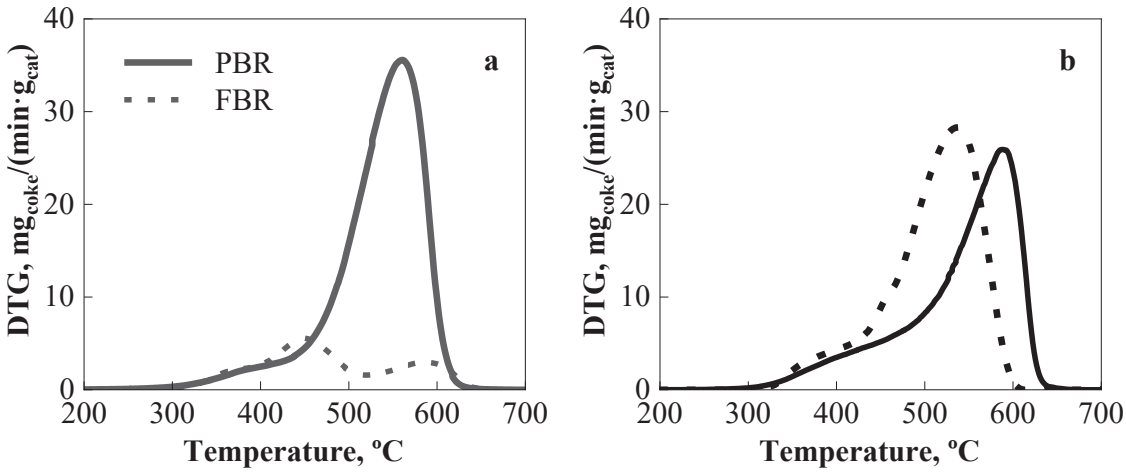

Fig. 10. TPO profiles for the catalyst used in the SR (a) and SESR (b) runs in PBR (solid lines) or FBR (dashed lines).

Table 3
Total coke and coke fractions content (wt%), and fraction of LT-coke deposited on the catalyst for SR and SESR runs with both reactor types.

Reactor type	Run	Coke content, wt%			LT-coke fraction
		LT-coke	HT-coke	Total	
PBR	SR	7.9	64.7	72.6	10.8
	SESR	15.0	49.6	64.6	23.3
FBR	SR	12.2	5.0	17.2	70.7
	SESR	13.6	43.9	57.5	23.7

3.2.4. *Structure of coke*

Fig. 12 shows the Raman spectra of the used catalysts. All the samples show the typical G (1593 cm^{-1}) and D (1343 cm^{-1}) bands attributable to different carbon structures, and other minor bands are also inferred at around 1200 cm^{-1} (associated to C—H vibrations) and 1500 cm^{-1} (associated to amorphous carbon and denoted as D'). The spectra have been deconvoluted into these four bands in order to have a better interpretation based on the D and G band widths and intensity ratios between G and D or D' (summarized results in Table 4 and Fig. S4). The deconvolution results can be interpreted under these premises:

- Smaller D and G band widths are related to more ordered and/or more homogeneous structures [62].
- The D/G band ratio is related to the degree of order or "graphitization" of the carbon structure, but the interpretation depends on the nature of the carbon structures. As observed by means of SEM, the coke is composed of amorphous carbon and carbon nanostructures (filaments and spheres). These carbon nanostructures typically have more intense D bands [63–65], and therefore a higher D/G intensity or area ratio would indicate the presence of these structures (together with the observation of smaller D and G band widths).

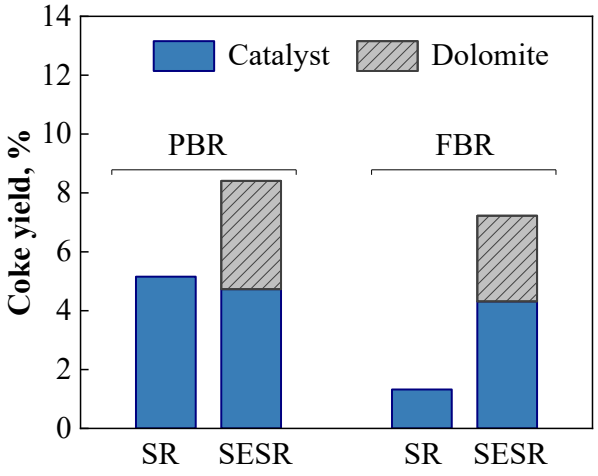

Fig. 11. Comparison of coke yields on catalyst and sorbent in SR and SESR runs with both reactor types.

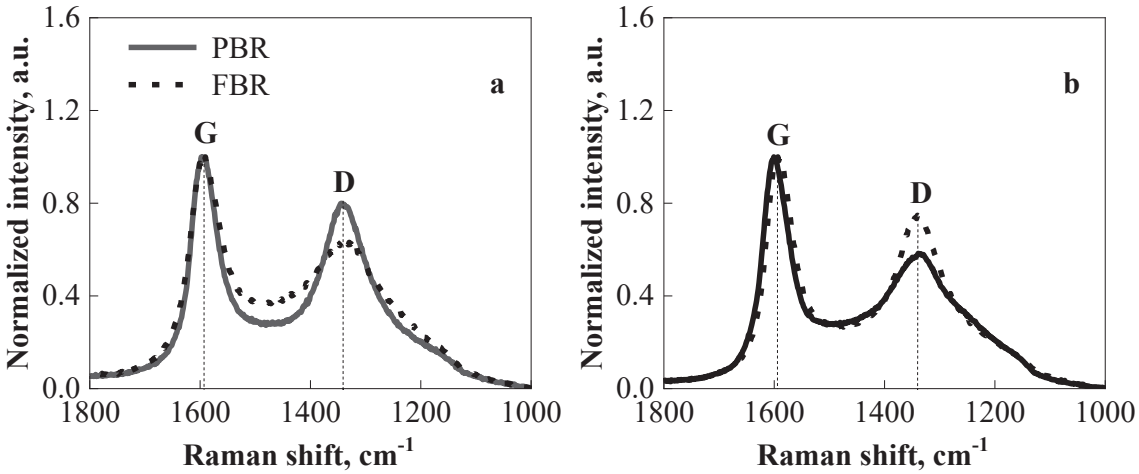

Fig. 12. Raman spectra of the catalyst used in the SR (a) and SESR (b) runs in PBR (solid lines) or FBR (dashed lines).

Table 4
Results of Raman spectra deconvolutions for the used catalysts.

Run	Reactor type	D band width	G band width	A_D/A_G [1]	I_D/I_G [2]	$A_{D'}/A_G$ [1]	$I_{D'}/I_G$ [2]
SR	PBR	108	52.7	1.62	0.788	0.420	0.153
	FBR	152	62.3	1.54	0.628	0.599	0.210
SESR	PBR	142	52.9	1.50	0.558	0.450	0.152
	FBR	112	53.9	1.49	0.718	0.392	0.145

[1]Calculated from the deconvoluted band areas.
[2]Calculated from the deconvoluted band height.

- The D'/G ratio gives a direct indicator of the relative content of amorphous carbon [63], and so as the D' band increases, the sample would have more amorphous carbon structures (together with the increase in the D band width).

Based on these premises and the deconvolution results, the coke formed in the SR in the PBR has a more ordered structure (higher D/G ratio and lower D band width) with less relative content of amorphous carbon structures (lower D'/G ratio) than that formed in the FBR. Contrariwise, the coke formed in the SESR in the FBR has a more ordered structure (higher D/G ratio and lower D band width) than that formed in the PBR, while the relative content of amorphous carbon structures is slightly lower. In any case, the coke formed in the SESR in both reactors has lower D'/G ratios than that formed in the SR in the FBR and smaller D band widths, which indicates that the coke formed in the SESR is more structured than that formed in the SR in the FBR. These observations are consistent with the SEM and TPO results that evidence a high presence of carbon filaments and spheres in the coke formed in the SR in the PBR, whereas that formed in the FBR is mostly amorphous carbon with low presence of carbon filaments. Similarly, the coke formed in the SESR in both reactors is mostly composed of carbon filaments, and these results confirm that the carbon filaments formed in the FBR are more structured than those formed in the PBR. Interestingly, the D'/G ratio calculated from the deconvolutions are linearly correlated with the combustion temperature corresponding to the maximum TPO peak (Fig. S5). This confirms that the combustion behavior is mostly related to the carbon structure nature.

The coke deposited on the sorbent was also analyzed by Raman spectroscopy (Fig. S6, Table S2), and the results indicate that this coke is composed of amorphous carbon (large D and G band widths and high D'/G ratios). This is also confirmed by the low temperature combustion determined by TPO analysis (Fig. S3), which is consistent with that of amorphous carbon structures.

4. Discussion

The results show that the fluid dynamic regime in the reactor significantly affects the oxygenates conversion, products yields and catalyst stability in the SR and SESR of raw bio-oil. Presumably, the bubbling and slugging phenomena may take place in the fluidized regime causing a fraction of the gas feed bypasses the catalyst particles and remains unreacted, which lowers the conversion and products yields. Likewise, both the fluid dynamic regime in the reactor and the reforming strategy (SR or SESR) greatly affects coke deposition (quantity and nature) that is related with the catalyst stability. This section mainly discusses this latter complex effect on the coke formation and incidence on the catalyst deactivation.

In general, coke is deposited on the external and internal surface of the $NiAl_2O_4$ spinel derived catalyst particles. The internal coke is related to amorphous carbon (LT-coke) formed from the oxygenates decomposition/cracking reaction whereas the external coke is related to developed carbon structures of carbon filaments and spheres (HT-coke) mostly formed from CH_4/hydrocarbons decomposition and Boudouard reactions.

In the SR runs, coke is deposited on both the external and internal surfaces of the catalyst particles in the PBR, whereas coke is preferentially deposited on the internal surface of the catalyst particles in the FBR. This difference on the preferential location of coke in the catalyst particles may be due to a phenomenon of catalyst "rejuvenation" in the FBR, which consists of favoring the coke gasification on the external surface because the particles are constantly moving in the bed, being in contact with a gaseous stream that favors its partial gasification and/or hinders the development of carbon filaments. Likewise, the external coke formed in the PBR is composed of carbon filaments and spheres, whereas that formed in the FBR is composed of solely carbon filaments. The formation of carbon spheres may be due to the favored development of these carbon structures in a static bed, whereas the moving particles in the FBR partially stop this development together with the occurrence of the "rejuvenation" phenomenon. The results confirm that the use of a FBR is adequate to stop the formation of HT-coke.

In the SESR runs, the presence of dolomite has different effects on the coke deposition according to the reactor type. In the PBR, dolomite presumably acts as a guard catalyst as the yield of coke on the catalyst decreases. Dolomite is able to catalyze the oxygenates decomposition/cracking reaction [53,54], thus competing with the Ni catalyst, and then part of the carbon fed remains as amorphous carbon (LT-coke) on the dolomite. Likewise, dolomite contribute to prevent the formation of carbon spheres in the duration of the reaction run tested in this work, which contributes to prolong the period of pseudo-stable activity in comparison with the SR process. This may be due to fact that this HT-

coke mainly comes from the products (negligible at the beginning of the reaction run because the CO_2 capture shifts the reactions equilibria towards the formation of H_2 and CO_2), which slows down the development of carbon structures. In the FBR, the presence of dolomite seems to favor the formation of carbon filaments (HT-coke) in comparison with the SR process, apparently lessening the effect of dolomite as a guard catalyst that occurs in the PBR. This effect of dolomite in the FBR may be due to two phenomena: i) dolomite favors the formation of carbon filaments from CH_4, hydrocarbons and CO originated from oxygenates decomposition/cracking reaction in the presence of dolomite, and the vigorous contact between dolomite and all catalyst particles in the FBR accelerates the mechanism of formation of these filaments upon the catalyst; ii) moreover, dolomite, especially when saturated, competes for the water adsorption preventing the "rejuvenation" effect expected in the FBR.

The correlation between the coke nature/quantification and the catalyst deactivation is unclear for all the scenarios studied in this work. Presumably, the formation of LT-coke (amorphous carbon) may contribute to block the Ni sites in the internal surface of the catalyst particles in the SR of bio-oil in the FBR, which causes a slow deactivation while a major part of the Ni sites in the external surface remains available for the reaction. However, the faster catalyst deactivation in the PBR may be related to the formation of carbon spheres (HT-coke) because these structures may encapsulate Ni sites [66] and their volume may block the access to the pores. Although carbon filaments (also part of the HT-coke) are commonly regarded as non-deactivated coke species because they typically follow a tip-growth mechanism, a base-growth mechanism is also likely to take place that can cause catalyst deactivation [66]. Thus, it is probably that the formation mechanism of carbon filaments has changed to a base-growth mechanism in the SESR process, in which Ni sites remain attached to the support and the filaments grow from them causing an encapsulation. Thus, the HT-coke composed of carbon filaments or spheres may cause catalyst deactivation depending on the growth mechanism.

It is interesting to highlight the good prospects of the system formed by $NiAl_2O4$ derived catalyst and dolomite for the cyclic operation required by the SESR process. Thus, in previous works [24,67] the regenerability of the $NiAl_2O_4$-derived catalyst under severe coke combustion conditions (850 °C) was revealed. At this temperature, not only the complete removal of the coke but also the complete reconstruction of the spinel structure is achieved, which is key for the complete recovery of its activity for the reforming of bio-oil oxygenates after the subsequent reduction of the spinel. Besides, by carbonation/decarbonation cycles in thermobalance (Fig. S7), it has been proven that the dolomite used in this study has a high stability for CO_2 capture, so that its capture capacity decreases from 42 gCO_2/(100 g dolomite) to 41 and 39 gCO_2/(100 g dolomite) after 5 and 10 cycles, respectively. Therefore, the $NiAl_2O_4$ spinel-derived catalyst is suitable for its use in bio-oil SESR, since the catalyst/sorbent bed can be jointly regenerated together at elevated temperature to recover both catalytic activity and CO_2 capture capacity. Therefore, a regeneration strategy has to be established, which we recommend to be with moving bed units. For dolomite, it must be assumed that CO_2 adsorption capacity is irreversibly lost, replacing a purge stream from the reactor with a fresh dolomite stream (low cost material). Furthermore, the purge dolomite will be a non-hazardous waste that can be used in construction.

5. Conclusions

The results prove the capacity of a Ni/Al_2O_3 catalyst prepared from a $NiAl_2O_4$ spinel to produce H_2 from raw bio-oil with in situ CO_2 capture using dolomite as a sorbent (SESR process). The good performance of this catalyst is due to homogeneous Ni sites distribution on the Al_2O_3 support, although the catalyst lifetime depends on the catalyst deactivation by coke. The use of various characterization techniques for analyzing the spent catalysts has been valuable to understand the effect of the rector type and the presence of dolomite on the coke quantity, nature and role on the catalyst deactivation.

The performance of the FBR is slightly inferior than that of the PBR for both SR and SESR processes, which is due to the less efficient contact between the gas fluid and catalyst particles causing a decrease in the oxygenates conversion and coke formation. The initial oxygenates conversion is almost complete in PBR and of 88 % in FBR, with H_2 yields of 80 % and 69 % in the PBR and FBR, respectively, for the SR process, and 99 % and 92 % during the CO_2 capture period (of 30 min duration) of the SESR runs in the PBR and FBR, respectively.

The catalyst deactivation rate in the SR runs is, however, slower in the FBR than in the PBR possibly due to rejuvenation of the catalyst surface because the particles movement may favor the coke gasification. This phenomenon has a significant incidence on the nature of coke deposited on the catalyst particles as the growth of carbon filaments is attenuated on the external surface, whereas the amorphous carbon formation in the internal porous structure is unaffected. This phenomenon does not take place in the PBR, which leads to more developed structures on the catalyst surface such as carbon filaments and spheres. The progressive formation of carbon spheres throughout the bed may be responsible of the catalyst deactivation as they may encapsulate Ni sites and block the access to mesopores.

The presence of dolomite in the bed prolongs the period of stable catalyst activity although the subsequent deactivation is slightly faster in both reactors in comparison with the SR process, more noticeably in the FBR. The effect of dolomite on the coke quantity and nature depends on the reactor type. In the PBR, dolomite acts mainly as a guard catalyst, slightly decreasing the total coke content on the catalyst and changing the coke nature to a combination of amorphous and filamentous carbons, preventing the formation of carbon spheres. The increase in the fraction of amorphous carbon may be responsible of the catalyst deactivation by blocking the surface of Ni sites. On the other hand, in the FBR, the presence of dolomite favors the formation of carbon filaments possibly due to the vigorous contact between dolomite and catalyst particles to favor the coke formation mechanisms, as dolomite favors oxygenates descomposition/cracking reaction forming filamentous coke precursors (such as CH_4 and hydrocarbons) and competes to adsorb water preventing coke gasification on the catalyst.

Attending to the interest of the FBR for the scale-up of the SR and SESR of raw bio-oil processes, the characteristics of the coke deactivation of the $NiAl_2O_4$ derived catalyst and of the coke deposition on the dolomite in this reactor should be considered in order to establish the regeneration strategy and the design of a reactor-regenerator system that will keep the H_2 production constant.

Declaration of Competing Interest

The authors declare that they have no known competing financial interests or personal relationships that could have appeared to influence the work reported in this paper.

Data availability

No data was used for the research described in the article.

Acknowledgements

This work has been carried out with the financial support of the grant RTI2018-100771-B-I00 and PID2021-127005OB-I00 funded by MCIN/AEI/10.13039/501100011033 and by "ERDF A way of making Europe", the European Commission (HORIZON H2020-MSCA RISE 2018. Contract No. 823745) and the Department of Education, Universities and Investigation of Basque Government (Project IT1645-22 and PhD grant PRE_2021_2_0147 for L. Landa). The authors thank for technical and human support provided by SGIker (UPV/EHU/ERDF, EU), and to Calcinor S.A. for supplying the dolomite.

Appendix A. Supplementary data

Supplementary data to this article can be found online at https://doi.org/10.1016/j.cej.2023.141494.

References

[1] Renewables – Fuels & Technologies – IEA, (n.d.). https://www.iea.org/fuels-and-technologies/renewables (accessed September 26, 2022).

[2] Z. Abdin, A. Zafaranloo, A. Rafiee, W. Mérida, W. Lipiński, K.R. Khalilpour, Hydrogen as an energy vector, Renew. Sustain. Energy Rev. 120 (2020), 109620, https://doi.org/10.1016/j.rser.2019.109620.

[3] T. Lepage, M. Kammoun, Q. Schmetz, A. Richel, Biomass-to-hydrogen: A review of main routes production, processes evaluation and techno-economical assessment, Biomass Bioenergy 144 (2021), 105920, https://doi.org/10.1016/j.biombioe.2020.105920.

[4] C. Wang, X. Zhang, Q. Liu, Q. Zhang, L. Chen, L. Ma, A review of conversion of lignocellulose biomass to liquid transport fuels by integrated refining strategies, Fuel Process. Technol. 208 (2020), 106485, https://doi.org/10.1016/j.fuproc.2020.106485.

[5] B.V. Ayodele, M.A. Alsaffar, S.I. Mustapa, A. Adesina, R. Kanthasamy, T. Witoon, S. Abdullah, Process intensification of hydrogen production by catalytic steam methane reforming: Performance analysis of multilayer perceptron-artificial neural networks and nonlinear response surface techniques, Process Saf. Environ. Prot. 156 (2021) 315–329, https://doi.org/10.1016/j.psep.2021.10.016.

[6] T. Shan Ahamed, S. Anto, T. Mathimani, K. Brindhadevi, A. Pugazhendhi, Upgrading of bio-oil from thermochemical conversion of various biomass – mechanism, challenges and opportunities, Fuel 287 (2021), 119329, https://doi.org/10.1016/j.fuel.2020.119329.

[7] G. Lopez, L. Santamaria, A. Lemonidou, S. Zhang, C. Wu, A.T. Sipra, N. Gao, Hydrogen generation from biomass by pyrolysis, Nat. Rev. Methods Prim. 2 (2022) 1–13, https://doi.org/10.1038/s43586-022-00097-8.

[8] H.A. Baloch, S. Nizamuddin, M.T.H. Siddiqui, S. Riaz, A.S. Jatoi, D.K. Dumbre, N. M. Mubarak, M.P. Srinivasan, G.J. Griffin, Recent advances in production and upgrading of bio-oil from biomass: a critical overview, J. Environ. Chem. Eng. 6 (2018) 5101–5118, https://doi.org/10.1016/j.jece.2018.07.050.

[9] D. Lee, H. Nam, M. Won Seo, S. Hoon Lee, D. Tokmurzin, S. Wang, Y.K. Park, Recent progress in the catalytic thermochemical conversion process of biomass for biofuels, Chem. Eng. J. 447 (2022), 137501, https://doi.org/10.1016/j.cej.2022.137501.

[10] B. Valle, N. García-Gómez, A. Arandia, A. Remiro, J. Bilbao, A.G. Gayubo, Effect of phenols extraction on the behavior of Ni-spinel derived catalyst for raw bio-oil steam reforming, Int. J. Hydrogen Energy. 44 (2019) 12593–12603, https://doi.org/10.1016/j.ijhydene.2018.12.057.

[11] Z. Zhao, Y.A. Situmorang, P. An, N. Chaihad, J. Wang, X. Hao, G. Xu, A. Abudula, G. Guan, Hydrogen production from catalytic steam reforming of bio-oils: a critical review, Chem. Eng. Technol. 43 (2020) 625–640, https://doi.org/10.1002/ceat.201900487.

[12] N. García-Gómez, J. Valecillos, A. Remiro, B. Valle, J. Bilbao, A.G. Gayubo, Effect of reaction conditions on the deactivation by coke of a $NiAl_2O_4$ spinel derived catalyst in the steam reforming of bio-oil, Appl. Catal. B Environ. 297 (2021), 120445, https://doi.org/10.1016/j.apcatb.2021.120445.

[13] R. Trane, S. Dahl, M.S. Skjøth-Rasmussen, A.D. Jensen, Catalytic steam reforming of bio-oil, Int. J. Hydrogen Energy. 37 (2012) 6447–6472, https://doi.org/10.1016/j.ijhydene.2012.01.023.

[14] A. Pafili, N.D. Charisiou, S.L. Douvartzides, G.I. Siakavelas, W. Wang, G. Liu, V. G. Papadakis, M.A. Goula, Recent progress in the steam reforming of bio-oil for hydrogen production: A review of operating parameters, catalytic systems and technological innovations, Catalysts 11 (2021) 1526, https://doi.org/10.3390/catal11121526.

[15] A. Di Giuliano, K. Gallucci, Sorption enhanced steam methane reforming based on nickel and calcium looping: a review, Chem. Eng. Process. - Process Intensif. 130 (2018) 240–252, https://doi.org/10.1016/j.cep.2018.06.021.

[16] X. Ma, Y. Li, X. Huang, T. Feng, M. Mu, Sorption-enhanced reaction process using advanced Ca-based sorbents for low-carbon hydrogen production, Process Saf. Environ. Prot. 155 (2021) 325–342, https://doi.org/10.1016/j.psep.2021.09.009.

[17] I.P. Lazzarotto, S.D. Ferreira, J. Junges, G.R. Bassanesi, C. Manera, D. Perondi, M. Godinho, The role of CaO in the steam gasification of plastic wastes recovered from the municipal solid waste in a fluidized bed reactor, Process Saf. Environ. Prot. 140 (2020) 60–67, https://doi.org/10.1016/j.psep.2020.04.009.

[18] P. Teixeira, C. Bacariza, P. Correia, C.I.C. Pinheiro, I. Cabrita, Hydrogen production with in situ CO_2 capture at high and medium temperatures using solid sorbents, Energies 15 (2022) 4039, https://doi.org/10.3390/en15114039.

[19] S. Masoudi Soltani, A. Lahiri, H. Bahzad, P. Clough, M. Gorbounov, Y. Yan, Sorption-enhanced steam methane reforming for combined CO_2 capture and hydrogen production: A state-of-the-art review, Carbon Capture Sci. Technol. 1 (2021), 100003, https://doi.org/10.1016/j.ccst.2021.100003.

[20] K.S. Ng, N. Zhang, J. Sadhukhan, Techno-economic analysis of polygeneration systems with carbon capture and storage and CO_2 reuse, Chem. Eng. J. 219 (2013) 96–108, https://doi.org/10.1016/j.cej.2012.12.082.

[21] Y. Zhang, T.R. Brown, G. Hu, R.C. Brown, Techno-economic analysis of two bio-oil upgrading pathways, Chem. Eng. J. 225 (2013) 895–904, https://doi.org/10.1016/j.cej.2013.01.030.

[22] Z. Wang, Y. Pan, T. Dong, X. Zhu, T. Kan, L. Yuan, Y. Torimoto, M. Sadakata, Q. Li, Production of hydrogen from catalytic steam reforming of bio-oil using C12A7-O^--based catalysts, Appl. Catal. A Gen. 320 (2007) 24–34, https://doi.org/10.1016/j.apcata.2006.12.003.

[23] P. Lan, Q. Xu, M. Zhou, L. Lan, S. Zhang, Y. Yan, Catalytic steam reforming of fast pyrolysis bio-oil in fixed bed and fluidized bed reactors, Chem. Eng. Technol. 33 (2010) 2021–2028, https://doi.org/10.1002/ceat.201000169.

[24] A. Remiro, A. Arandia, L. Oar-Arteta, J. Bilbao, A.G. Gayubo, Regeneration of $NiAl_2O_4$ spinel type catalysts used in the reforming of raw bio-oil, Appl. Catal. B Environ. 237 (2018) 353–365, https://doi.org/10.1016/j.apcatb.2018.06.005.

[25] S. Czernik, R. French, C. Feik, E. Chornet, Hydrogen by catalytic steam reforming of liquid byproducts from biomass thermoconversion processes, Ind. Eng. Chem. Res. 41 (2002) 4209–4215, https://doi.org/10.1021/ie020107q.

[26] J. Remón, J.A. Medrano, F. Bimbela, L. García, J. Arauzo, Ni/Al–Mg–O solids modified with Co or Cu for the catalytic steam reforming of bio-oil, Appl. Catal. B Environ. 132–133 (2013) 433–444, https://doi.org/10.1016/j.apcatb.2012.12.015.

[27] P. Fu, W. Yi, Z. Li, X. Bai, A. Zhang, Y. Li, Z. Li, Investigation on hydrogen production by catalytic steam reforming of maize stalk fast pyrolysis bio-oil, Int. J. Hydrogen Energy. 39 (2014) 13962–13971, https://doi.org/10.1016/j.ijhydene.2014.06.165.

[28] M. Abbasi, M. Farniaei, S. Abbasi, Enhancement of hydrogen production by fluidization in industrial-scale steam reformers, Theor Found Chem Eng 52 (3) (2018) 416–428, https://doi.org/10.1134/S0040579518030016.

[29] T. Papalas, A.N. Antzaras, A.A. Lemonidou, Intensified steam methane reforming coupled with Ca-Ni looping in a dual fluidized bed reactor system: A conceptual design, Chem. Eng. J. 382 (2020), 122993, https://doi.org/10.1016/j.cej.2019.122993.

[30] A. Effendi, Z.G. Zhang, K. Hellgardt, K. Honda, T. Yoshida, Steam reforming of a clean model biogas over Ni/Al_2O_3 in fluidized- and fixed-bed reactors, Catal. Today. 77 (2002) 181–189, https://doi.org/10.1016/s0920-5861(02)00244-4.

[31] A. Kumar, R. Singh, A.S.K. Sinha, Catalyst modification strategies to enhance the catalyst activity and stability during steam reforming of acetic acid for hydrogen production, Int. J. Hydrogen Energy. 44 (2019) 12983–13010, https://doi.org/10.1016/j.ijhydene.2019.03.136.

[32] J. Remón, F. Broust, J. Valette, Y. Chhiti, I. Alava, A.R. Fernandez-Akarregi, J. Arauzo, L. Garcia, Production of a hydrogen-rich gas from fast pyrolysis bio-oils: Comparison between homogeneous and catalytic steam reforming routes, Int. J. Hydrogen Energy. 39 (2014) 171–182, https://doi.org/10.1016/j.ijhydene.2013.10.025.

[33] P.N. Kechagiopoulos, S.S. Voutetakis, A.A. Lemonidou, I.A. Vasalos, Hydrogen production via reforming of the aqueous phase of bio-oil over Ni/olivine catalysts in a spouted bed reactor, Ind. Eng. Chem. Res. 48 (2009) 1400–1408, https://doi.org/10.1021/ie8013378.

[34] V. Palma, C. Ruocco, E. Meloni, A. Ricca, Oxidative reforming of ethanol over CeO_2-SiO_2 based catalysts in a fluidized bed reactor, Chem. Eng. Process. - Process Intensif. 124 (2018) 319–327, https://doi.org/10.1016/j.cep.2017.08.010.

[35] D. Kunii, O. Levenspiel, Bubbling bed model for kinetic processes in fluidized beds: gas-solid mass and heat transfer and catalytic reactions, Ind. Eng. Chem. Process Des. Dev. 7 (1968) 481–492, https://doi.org/10.1021/i260028a001.

[36] H.K. Rusten, E. Ochoa-Fernández, H. Lindborg, D. Chen, H.A. Jakobsen, Hydrogen production by sorption-enhanced steam methane reforming using lithium oxides as CO_2-acceptor, Ind. Eng. Chem. Res. 46 (2007) 8729–8737, https://doi.org/10.1021/ie070770k.

[37] Y. Shi, X. Du, L. Yang, Y. Sun, Y. Yang, Experiments on hydrogen production from methanol steam reforming in fluidized bed reactor, Int. J. Hydrogen Energy. 38 (2013) 13974–13981, https://doi.org/10.1016/j.ijhydene.2013.08.073.

[38] E. Fernandez, M. Amutio, M. Artetxe, A. Arregi, L. Santamaria, G. Lopez, J. Bilbao, M. Olazar, Assessment of product yields and catalyst deactivation in fixed and fluidized bed reactors in the steam reforming of biomass pyrolysis volatiles, Process Saf. Environ. Prot. 145 (2021) 52–62, https://doi.org/10.1016/j.psep.2020.07.039.

[39] A. Ochoa, B. Aramburu, B. Valle, D.E. Resasco, J. Bilbao, A.G. Gayubo, P. Castaño, Role of oxygenates and effect of operating conditions in the deactivation of a Ni supported catalyst during the steam reforming of bio-oil, Green Chem. 19 (2017) 4315–4333, https://doi.org/10.1039/c7gc01432e.

[40] H. Sun, C. Wu, B. Shen, X. Zhang, Y. Zhang, J. Huang, Progress in the development and application of CaO-based adsorbents for CO_2 capture—a review, Mater. Today Sustain. 1–2 (2018) 1–27, https://doi.org/10.1016/j.mtsust.2018.08.001.

[41] Y. Wang, M.Z. Memon, M.A. Seelro, W. Fu, Y. Gao, Y. Dong, G. Ji, A review of CO_2 sorbents for promoting hydrogen production in the sorption-enhanced steam reforming process, Int. J. Hydrogen Energy. 46 (2021) 23358–23379, https://doi.org/10.1016/j.ijhydene.2021.01.206.

[42] S. Rodríguez, A. Capa, R. García, D. Chen, F. Rubiera, C. Pevida, M.V. Gil, Blends of bio-oil/biogas model compounds for high-purity H_2 production by sorption enhanced steam reforming (SESR): Experimental study and energy analysis, Chem. Eng. J. 432 (2022), 134396, https://doi.org/10.1016/j.cej.2021.134396.

[43] A. Arandia, A. Remiro, B. Valle, J. Bilbao, A.G. Gayubo, Deactivation of Ni spinel derived catalyst during the oxidative steam reforming of raw bio-oil, Fuel 276 (2020), 117995, https://doi.org/10.1016/j.fuel.2020.117995.

[44] L. Landa, A. Remiro, J. Valecillos, B. Valle, J. Bilbao, A.G. Gayubo, Unveiling the deactivation by coke of $NiAl_2O_4$ spinel derived catalysts in the bio-oil steam reforming: Role of individual oxygenates, Fuel 321 (2022), 124009, https://doi.org/10.1016/j.fuel.2022.124009.

[45] X. Hu, Z. Zhang, M. Gholizadeh, S. Zhang, C.H. Lam, Z. Xiong, Y. Wang, Coke formation during thermal treatment of bio-oil, Energy Fuel 34 (2020) 7863–7914, https://doi.org/10.1021/acs.energyfuels.0c01323.
[46] B. Valle, B. Aramburu, P.L. Benito, J. Bilbao, A.G. Gayubo, Biomass to hydrogen-rich gas via steam reforming of raw bio-oil over Ni/La_2O_3-αAl_2O_3 catalyst: Effect of space-time and steam-to-carbon ratio, Fuel 216 (2018) 445–455, https://doi.org/10.1016/j.fuel.2017.11.151.
[47] B. Valle, B. Aramburu, A. Remiro, A. Arandia, J. Bilbao, A.G. Gayubo, Optimal conditions of thermal treatment unit for the steam reforming of raw bio-oil in a continuous two-step reaction system, Chem. Eng. Trans. 57 (2017) 205–210, https://doi.org/10.3303/cet1757035.
[48] C. Montero, L. Oar-Arteta, A. Remiro, A. Arandia, J. Bilbao, A.G. Gayubo, Thermodynamic comparison between bio-oil and ethanol steam reforming, Int. J. Hydrogen Energy. 40 (2015) 15963–15971, https://doi.org/10.1016/j.ijhydene.2015.09.125.
[49] L. Landa, A. Remiro, R. de la Torre, R. Aguado, J. Bilbao, A.G. Gayubo, Global vision from the thermodynamics of the effect of the bio-oil composition and the reforming strategies in the H_2 production and the energy requirement, Energy Convers. Manag. 239 (2021), 114181, https://doi.org/10.1016/j.enconman.2021.114181.
[50] A. Ochoa, B. Valle, D.E. Resasco, J. Bilbao, A.G. Gayubo, P. Castaño, Temperature programmed oxidation coupled with in situ techniques reveal the nature and location of coke deposited on a Ni/La_2O_3-αAl_2O_3 catalyst in the steam reforming of bio-oil, ChemCatChem 10 (2018) 2311–2321, https://doi.org/10.1002/cctc.201701942.
[51] A. Ochoa, A. Arregi, M. Amutio, A.G. Gayubo, M. Olazar, J. Bilbao, P. Castaño, Coking and sintering progress of a Ni supported catalyst in the steam reforming of biomass pyrolysis volatiles, Appl. Catal. B Environ. 233 (2018) 289–300, https://doi.org/10.1016/j.apcatb.2018.04.002.
[52] A. Ochoa, J. Bilbao, A.G. Gayubo, P. Castaño, Coke formation and deactivation during catalytic reforming of biomass and waste pyrolysis products: A review, Renew. Sustain. Energy Rev. 119 (2020), 109600, https://doi.org/10.1016/j.rser.2019.109600.
[53] B. Valle, N. García-Gómez, A. Remiro, J. Bilbao, A.G. Gayubo, Dual catalyst-sorbent role of dolomite in the steam reforming of raw bio-oil for producing H_2-rich syngas, Fuel Process. Technol. 200 (2020), 106316, https://doi.org/10.1016/j.fuproc.2019.106316.
[54] N. García-Gómez, B. Valle, J. Valecillos, A. Remiro, J. Bilbao, A.G. Gayubo, Feasibility of online pre-reforming step with dolomite for improving Ni spinel catalyst stability in the steam reforming of raw bio-oil, Fuel Process. Technol. 215 (2021), 106769, https://doi.org/10.1016/j.fuproc.2021.106769.
[55] N. García-Gómez, J. Valecillos, B. Valle, A. Remiro, J. Bilbao, A.G. Gayubo, Combined effect of bio-oil composition and temperature on the stability of Ni spinel derived catalyst for hydrogen production by steam reforming, Fuel 326 (2022), 124966, https://doi.org/10.1016/j.fuel.2022.124966.
[56] Y. Hu, X. Li, L. Zhang, M. Zhou, G. Wang, Y. Zhang, C. Xi, S. Cao, Mesoporous alumina as a solid phase extraction adsorbent for the determination of abamectin and ivermectin in vegetables by liquid chromatography-tandem mass spectrometry, Anal. Methods. 6 (2014) 4734–4741, https://doi.org/10.1039/c4ay00107a.
[57] J.C. Acomb, C. Wu, P.T. Williams, Effect of growth temperature and feedstock: catalyst ratio on the production of carbon nanotubes and hydrogen from the pyrolysis of waste plastics, J. Anal. Appl. Pyrolysis. 113 (2015) 231–238, https://doi.org/10.1016/j.jaap.2015.01.012.
[58] S. Hu, L. He, Y. Wang, S. Su, L. Jiang, Q. Chen, Q. Liu, H. Chi, J. Xiang, L. Sun, Effects of oxygen species from Fe addition on promoting steam reforming of toluene over $Fe–Ni/Al_2O_3$ catalysts, Int. J. Hydrogen Energy. 41 (2016) 17967–17975, https://doi.org/10.1016/j.ijhydene.2016.07.271.
[59] L. He, G. Liao, S. Hu, L. Jiang, H. Han, H. Li, Q. Ren, M.E. Mostafa, X. Hu, Y. i. Wang, S. Su, J. Xiang, Effect of temperature on multiple competitive processes for co-production of carbon nanotubes and hydrogen during catalytic reforming of toluene, Fuel 264 (2020) 116749, https://doi.org/10.1016/j.fuel.2019.116749.
[60] L. He, G. Liao, H. Li, Q. Ren, S. Hu, H. Han, J. Xu, L. Jiang, S. Su, Y. Wang, J. Xiang, Evolution characteristics of different types of coke deposition during catalytic removal of biomass tar, J. Energy Inst. 93 (2020) 2497–2504, https://doi.org/10.1016/j.joei.2020.08.009.
[61] G. Giammaria, L. Lefferts, Catalytic effect of water on calcium carbonate decomposition, J. CO_2 Util. 33 (2019) 341–356, https://doi.org/10.1016/j.jcou.2019.06.017.
[62] K. Chen, H. Zhang, U.K. Ibrahim, W.Y. Xue, H. Liu, A. Guo, The quantitative assessment of coke morphology based on the Raman spectroscopic characterization of serial petroleum cokes, Fuel 246 (2019) 60–68, https://doi.org/10.1016/j.fuel.2019.02.096.
[63] Y.C. Choi, K.-I. Min, M.S. Jeong, Novel method of evaluating the purity of multiwall carbon nanotubes using raman spectroscopy, J. Nanomater. 2013 (2013) 1–6, https://doi.org/10.1155/2013/615915.
[64] K.L.A. Cao, A.M. Rahmatika, Y. Kitamoto, M.T.T. Nguyen, T. Ogi, Controllable synthesis of spherical carbon particles transition from dense to hollow structure derived from Kraft lignin, J. Colloid Interface Sci. 589 (2021) 252–263, https://doi.org/10.1016/j.jcis.2020.12.077.
[65] J.M. Ambriz-Torres, L.D. Lvova, C.J.G. García, P. Garnica-González, O. Aguilar-García, J.J. Contreras-Navarrete, Characterization and comparison of carbon structures synthesized from rubber waste and naphthalene, MRS Adv. 7 (2022) 945–949, https://doi.org/10.1557/s43580-022-00338-8.
[66] L. Chen, L.E. Noreña, J.A. Wang, R. Limas, U. Arellano, O.A.G. Vargas, Promoting role of amorphous carbon and carbon nanotubes growth modes of methane decomposition in one-pot catalytic approach, Catalyst 11 (2021) 1217, https://doi.org/10.3390/catal11101217.
[67] A. Arandia, A. Remiro, V. García, P. Castaño, J. Bilbao, A.G. Gayubo, Oxidative steam reforming of raw bio-oil over supported and bulk Ni catalysts for hydrogen production, Catalysts 8 (2018) 322, https://doi.org/10.3390/catal8080322.